Influence of an external voltage on the conductance through a quantum dot side-coupled to a short quantum wire

2005 J. Phys.: Condens. Matter 17 5987

(http://iopscience.iop.org/0953-8984/17/38/004)

INSTITUTE OF PHYSICS PUBLISHING JOURNAL OF PHYSICS: CONDENSED MATTER

J. Phys.: Condens. Matter **17** (2005) 5987–5995 doi:10.1088/0953-8984/17/38/004

Influence of an external voltage on the conductance through a quantum dot side-coupled to a short quantum wire

Zhi-Yong Zhang and Shi-Jie Xiong

Department of Physics, Nanjing University, Nanjing 210093, People's Republic of China

Received 28 September 2004, in final form 19 July 2005
Published 9 September 2005
Online at stacks.iop.org/JPhysCM/17/5987

Abstract

We investigate the influence of an external voltage V_0 on conductance G through a quantum dot (QD), which is side-coupled to a quantum wire of length L_W, whose two ends are weakly connected to leads. In our calculation, the poor man's scaling law and slave-boson mean-field method are employed. With V_0 increased, a series of resonant regions is formed and G exhibits different properties in and out of these regions, which is the universal result of the finite-size effect on the Kondo correlation. In symmetric structures, the would-be resonant regions corresponding to odd wavefunctions are removed. If the symmetry is broken by changing the QD position, those regions will be recovered. In two asymmetric structures with their wire lengths being L_W and $L_W + 1$, respectively, the two sets of resonant regions intersect with each other. These symmetry-related phenomena characterize side-coupled QD structures. With the barrier width increased, the number of resonant regions is increased, too.

1. Introduction

With the development of nanofabrication techniques, the interplay between electronic correlation and finite-size effect has attracted a lot of attention in the mesoscopic physics. When a quantum dot (QD) is connected to metallic leads, the coupling between the localized spin on the dot and conduction electrons results in the Kondo correlation, which is described by an energy scale T_K, the so-called Kondo temperature. If a dot is in the Kondo regime [1–5], the localized spin and conduction electrons form a spin singlet state, which yields the Abrikosov–Suhl resonance and profoundly affects the electronic transport. The dynamical correlation length of the spin singlet is related to T_K by $\xi_K = \hbar v_F / T_K$, with v_F the Fermi velocity [6]. However, if the dimension of a QD structure is shorter than ξ_K, the effective Kondo temperature T_K will deviate from the bare one (below, we use $T_K^{(0)}$ and $\xi_K^{(0)}$ to denote the bare characteristic scales), and at this time the finite-size effect plays an important role [7–13].

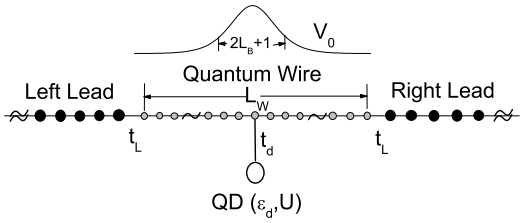

Figure 1. Schematic illustration of the structure.

Recently, Simon and Affleck have studied the transport properties of a structure where a QD is embedded in a quantum wire (QW), whose two ends are weakly connected to external leads [12]. Due to the finite wire length L_W, the local density of states (LDOS) of conduction electrons seen by the localized electron on the dot $\rho_s(\omega)$ has a series of peaks. If the peak distance $\Delta > T_K^{(0)}$, a great difference (usually several orders in magnitude) can be found between $T_K^{(R)}$ and $T_K^{(NR)}$, which are the corresponding T_K with the Fermi energy ϵ_F being resonant and non-resonant with LDOS peaks, respectively [11, 12]. This point can be seen clearly from the poor man's scaling law (PMSL) [14]. By applying a gate voltage on the wire, whether the structure is in or out of resonant regions can be artificially adjusted.

Although they are obtained from embedded QD structures, it looks reasonable that these results can also be found in a structure with the QD side-coupled to the wire. Of course, this point needs to be clarified. Meanwhile, in embedded QD structures, with the Kondo coupling J approaching zero, the wire is effectively cut into two parts, and with J increased the two parts are merged together, which leads to the doubling of the number of resonant regions when $T_K^{(0)}$ is enhanced from much smaller to much larger than Δ. Obviously, this phenomenon cannot be found in side-coupled QD structures. What characterizes the transport property through a side-coupled QD structure is a question that need to be answered. Furthermore, in [12], the gate voltage is assumed constant over the whole wire. If an external voltage V_0 is applied on the wire to form a potential barrier, with its width being shorter than L_W, what is the difference between this situation and that with constant gate voltage? The purpose of the present paper is to resolve these three problems.

For this reason, we assume a structure illustrated schematically in figure 1, obtain T_K qualitatively from PMSL [14], treat the Kondo correlation via the slave-boson mean-field (SBMF) method of Kotliar and Ruckenstein (KR) [15–17] and calculate the conductance G through the structure by the Landauer–Büttiker formula. With V_0 increased, a series of resonant regions is found, where Kondo-assisted tunnelling yields very small G values. Outside these regions, intrinsic structure of G is found due to the scattering at interfaces between the wire and leads. Here, the practical temperature T satisfies the relation $T_K^{(NR)} \ll T \ll T_K^{(R)}$. This is the universal result of the finite-size effect on the Kondo correlation. Consider the situation where the wire contains an odd number of sites: if the QD is side-coupled to the symmetric site the would-be resonant regions corresponding to odd wavefunctions are removed, but if the dot is side-coupled to one other site the symmetry is broken and those regions are recovered. In two asymmetric structures with their wire length being L_W and $L_W + 1$, respectively, the two sets of resonant regions intersect with each other. These symmetry-related phenomena characterize side-coupled QD structures. With V_0 constant over the wire, the $\rho_s(\omega)$ curve moves rigidly. If a potential barrier is formed in the wire, with its effective width being shorter than L_W, some peaks in the $\rho_s(\omega)$ curve are diminished and removed with V_0 increased, so that the number of resonant regions is decreased.

The organization of this paper is as follows. In section 2, the theoretical model and calculation method are illustrated. In section 3, the numerical results and the discussion on them are presented. A brief summary is given in section 4.

2. Model and formulas

In the present paper, we investigate the transport property of a QD, which is side-coupled to a short quantum wire, and study the influence of external voltage on its conductance. The structure is schematically illustrated in figure 1, where one dot, with a single-particle energy level ϵ_d and an on-site Coulomb interaction U, is connected to the QW by hopping integral t_d. The length of the QW is $L_{\rm W}$, whose two ends are weakly connected to leads via tunnelling matrix element $t_{\rm L}$. This mesoscopic system can be described by the following one-dimensional (1D) tight-binding Hamiltonian:

$$H = H_{\rm L} + H_{\rm W} + H_{\rm D} + H_{\rm LW} + H_{\rm DW}, \tag{1}$$

where the subscripts L, W and D stand for lead, wire and dot, respectively. Here

$$H_{\rm L} = -t\left[\sum_{i=-\infty,\sigma}^{-1} + \sum_{i=L_{\rm W}+1,\sigma}^{\infty}\right](c_{i\sigma}^{\dagger}c_{i+1\sigma} + {\rm H.c.}), \tag{2}$$

$$H_{\rm W} = \sum_{i=1,\sigma}^{L_{\rm W}} V_i c_{i\sigma}^{\dagger}c_{i\sigma} - t\sum_{i=1,\sigma}^{L_{\rm W}-1}(c_{i\sigma}^{\dagger}c_{i+1\sigma} + {\rm H.c.}), \tag{3}$$

$$H_{\rm D} = \epsilon_d \sum_{\sigma} c_{d\sigma}^{\dagger}c_{d\sigma} + U n_{d\uparrow}n_{d\downarrow}, \tag{4}$$

$$H_{\rm LW} = -t_{\rm L}\sum_{\sigma}(c_{0\sigma}^{\dagger}c_{1\sigma} + c_{L_{\rm W}\sigma}^{\dagger}c_{L_{\rm W}+1\sigma} + {\rm H.c.}) \tag{5}$$

and

$$H_{\rm DW} = -t_d\sum_{\sigma}(c_{d\sigma}^{\dagger}c_{s\sigma} + {\rm H.c.}). \tag{6}$$

Here $n_{d\sigma} = c_{d\sigma}^{\dagger}c_{d\sigma}$, with $\sigma = \uparrow$ or $\downarrow$, and the QD is connected to site s. The external voltage forms a potential barrier, and its centre coincides with the central site 'c' of the wire $V_i = V_0/\cosh^2(\frac{i-c}{L_{\rm B}})$, with $c = (L_{\rm W}+1)/2$. Here, the barrier tail in leads is neglected. As a comparison, the situation with constant external voltage $V_i = V_0$ is also considered in this paper.

When the dot is decoupled from the QW, the LDOS on site s can be obtained easily:

$$\rho_{\rm s}(\omega) = -\frac{1}{\pi}\,{\rm Im}\langle{\rm vac}|c_{\rm s}[\omega + {\rm i}\gamma - (H_{\rm L} + H_{\rm W} + H_{\rm LW})]^{-1}c_{\rm s}^{\dagger}|{\rm Vac}\rangle, \tag{7}$$

where ${\rm i} = \sqrt{-1}$, γ is introduced to denote the half width at half maximum of the spectrum lines in LDOS and $|{\rm Vac}\rangle$ is the vacuum state. Due to the spin degeneracy, the spin subscript is omitted in the above formula. When the QD is coupled with the QW, the correlation interaction plays an important role, and $T_{\rm K}$ can be obtained qualitatively from PMSL [12, 14]:

$$\frac{{\rm d}J}{{\rm d}\ln(D_0/\omega)} = \rho_{\rm s}(\omega)J^2, \tag{8}$$

where $D_0 = 2t$ is the original bandwidth, and the corresponding unrenormalized Kondo coupling is $J_0 = 2t_d^2\left(\frac{1}{-\epsilon_d} + \frac{1}{\epsilon_d+U}\right)$. $T_{\rm K}$ is defined as the specific ω value where the renormalized J equals unity. If $L_{\rm W} \to \infty$ and $V_0 = 0$, $T_{\rm K}^{(0)} = D_0\exp(-1/\lambda)$, with $\lambda = J_0/(2\pi t)$. This

expression is a little different from the exact one [6], but as a qualitative result, it is good enough.

To solve the Hamiltonian (1), we adopt the SBMF theory of KR [16, 18], which is a powerful nonperturbative tool to study the strongly correlated fermion system, and can give qualitatively correct results when the Kondo correlation is dealt with [10, 15]. In the framework of this approach, four auxiliary boson fields e, p_σ and d are introduced, which act as projection operators onto the empty, singly occupied and doubly occupied electronic states at the QD, respectively. To eliminate the unphysical states, three constraints have to be imposed: $\sum_\sigma p_\sigma^\dagger p_\sigma + e^\dagger e + d^\dagger d = 1$ and $c_{d\sigma}^\dagger c_{d\sigma} = p_\sigma^\dagger p_\sigma + d^\dagger d$. To obtain correct result in the noninteracting limit, the fermion operator $c_{d\sigma}$ should be replaced by $c_{d\sigma} z_\sigma$, with $z_\sigma = (1-d^\dagger d - p_\sigma^\dagger p_\sigma)^{-1/2}(e^\dagger p_\sigma + p_{\bar\sigma}^\dagger d)(1-e^\dagger e - p_{\bar\sigma}^\dagger p_{\bar\sigma})^{-1/2}$. Therefore the Hamiltonian (1) can be replaced by the following effective Hamiltonian:

$$H_{\rm eff} = H_{\rm L} + H_{\rm W} + \tilde H_{\rm D} + H_{\rm LW} + \tilde H_{\rm DW} + \lambda^{(1)}\left(\sum_\sigma p_\sigma^\dagger p_\sigma + e^\dagger e + d^\dagger d - 1\right) + \sum_\sigma \lambda_\sigma^{(2)}(c_{d\sigma}^\dagger c_{d\sigma} - p_\sigma^\dagger p_\sigma - d^\dagger d), \tag{9}$$

where the three constraints are incorporated by the Lagrange multipliers $\lambda^{(1)}$ and $\lambda_\sigma^{(2)}$. The original $H_{\rm D}$ and $H_{\rm DW}$ are replaced by

$$\tilde H_{\rm D} = \epsilon_d \sum_\sigma c_{d\sigma}^\dagger c_{d\sigma} + U d^\dagger d \tag{10}$$

and

$$\tilde H_{\rm DW} = -t_d \sum_\sigma (z_\sigma^\dagger c_{d\sigma}^\dagger c_{s\sigma} + {\rm H.c.}), \tag{11}$$

whereas $H_{\rm L}$, $H_{\rm W}$ and $H_{\rm LW}$ remain unchanged.

To solve the effective Hamiltonian (9) at finite temperature, we first replace the slave boson fields by their expectation values, then obtain the values of e, p_σ, d, $\lambda^{(1)}$ and $\lambda_\sigma^{(2)}$ by minimization of the corresponding free energy of the essentially noninteracting Hamiltonian (9) with respect to these parameters [17]. This is equivalent to the approach using the functional integral method combined with the saddle-point approximation, and leads to a set of self-consistent equations [16, 17]:

$$e^2 + 2p^2 + d^2 = 1, \tag{12}$$

$$\sum_m n_{\rm F}(\epsilon_m)\langle m|c_d^\dagger c_d|m\rangle - p^2 - d^2 = 0, \tag{13}$$

$$-2t_d \sum_m n_{\rm F}(\epsilon_m)\langle m|c_d^\dagger c_{\rm s} + {\rm H.c.}|m\rangle \frac{\partial z}{\partial(e^2)} + \lambda^{(1)} = 0, \tag{14}$$

$$-t_d \sum_m n_{\rm F}(\epsilon_m)\langle m|c_d^\dagger c_{\rm s} + {\rm H.c.}|m\rangle \frac{\partial z}{\partial(p^2)} + \lambda^{(1)} - \lambda^{(2)} = 0 \tag{15}$$

and

$$-2t_d \sum_m n_{\rm F}(\epsilon_m)\langle m|c_d^\dagger c_{\rm s} + {\rm H.c.}|m\rangle \frac{\partial z}{\partial(d^2)} + \lambda^{(1)} - 2\lambda^{(2)} + U = 0, \tag{16}$$

where $n_{\rm F}(\epsilon_m)$ is the Fermi distribution function $n_{\rm F}(\epsilon_m) = 1/(1+{\rm e}^{\beta(\epsilon_m-\epsilon_{\rm F})})$, with $\beta = 1/T$ the inverse temperature. In the present paper, we always set $\epsilon_{\rm F} = 0$. Because of the spin-degeneracy, only five variational parameters are independent. They are e, p, d, $\lambda^{(1)}$ and $\lambda^{(2)}$. Based on the same reason, in writing the above self-consistent equations, the spin notations of fermion operators are omitted.

To self-consistently solve these equations, we have to calculate the expectation values such as $\langle m|c_j^\dagger c_i|m\rangle$, with $|m\rangle$ the single-particle eigenstate corresponding to a certain set of variational parameters, then update the variational parameters from the above self-consistent equations, and repeat these two steps until numeric convergence is reached. The introduction of an external voltage makes it not easy to write analytic expressions of those expectation values, and they are obtained via numeric calculations. In practical calculations, the numeric diagonalization can be performed only in a finite cluster. Here, the QW, together with the side-coupled QD, is located at the centre of the cluster. At zero temperature, if the cluster size is much larger than ξ_K, the results obtained from the cluster calculation should be identical with those from the original system [8, 10]. Whereas at finite temperature, the required cluster size is relative short compared with that at zero temperature.

As soon as the five variational parameters are obtained, the conductance G through the structure can be obtained from the Landauer–Büttiker (LB) formula:

$$G = 2\int -\frac{\partial n_F(\epsilon)}{\partial \epsilon}|T_r(\epsilon)|^2\,\mathrm{d}\epsilon, \tag{17}$$

since the effective Hamiltonian (9) is essentially noninteracting [20]. Here, the factor 2 accounts for the spin degeneracy and $T_r(\epsilon)$ is the transmission coefficient of an incident electron with energy ϵ. For the effectively noninteracting tight-binding Hamiltonian (9), T_r can be calculated straightforwardly from the transfer matrix (TM) method [9, 12, 19].

3. Results and discussion

In the following calculation, we always set $t = 1$, $\epsilon_d = -0.7$, $U = 1.4$, $t_d = 0.5$, $t_L = 0.5$, $T = 10^{-3}$ and $\gamma = t_L^2/(2L_W)$. Consequently, $T_K^{(0)} = 2.46 \times 10^{-2}$ and $\xi_K^{(0)} = 81.3$. When the dot is side-coupled to the wire, to take the Kondo correlation into account, in calculating G, the total cluster size is set as 600, which is much longer than $\xi_K^{(0)}$. Although ξ_K is usually different from $\xi_K^{(0)}$, at $T = 10^{-3}$, this cluster size can always guarantee the numeric convergence. Whereas in calculating ρ_s with the dot decoupled, a cluster with 2000 sites is diagonalized to guarantee the smoothness of obtained curves. In the present paper, three different situations are considered. (i) $L_W = 19$ and the QD is side-coupled to the site $s = 10$. This situation is symmetric in structure and is labelled as 'L_W19s'. (ii) $L_W = 20$ and $s = 10$. This situation is labelled as 'L_W20'. (iii) $L_W = 19$ and $s = 9$. We label it as 'L_W19a'. In the second and third situations, the structure is asymmetrical.

Figures 2(a)–(c) illustrate the variations of $\rho_s(\epsilon_F)$, T_K and G versus V_0, respectively, with $L_B = 5$. In 'L_W19s', two high peaks appear in the $\rho_s(\epsilon_F)$–V_0 curve, and a low one is located at $V_0 \sim 2.35t$. Correspondingly, T_K also shows two high peaks in the two major resonant regions, with their peak values $T_K^{(R)} \sim 0.010$ and 0.016, respectively, and a low one, about 7.7×10^{-6}. In the non-resonant regions, $T_K^{(NR)} \sim 2.1 \times 10^{-10}$, 1.1×10^{-7} and 4.0×10^{-8} at the tips. Here, linear–log axes are used to plot the T_K and G curves. In figure 2(b), the position of T is noted as a horizontal line, and as we can see the relation $T_K^{(NR)} \ll T \ll T_K^{(R)}$ is satisfied. Consequently, in the resonant regions, the Kondo-assisted tunnelling plays an important role, and G takes a very small value since the QD is side-coupled to the wire [21]. In the non-resonant regions, the electronic interaction is perturbative, and G exhibits intrinsic structure caused by the scattering at the interfaces between the wire and leads. Meanwhile, a shallow dip related to the low $\rho_s(\epsilon_F)$ peak is found in the G curve.

With $V_0 = 0$, $\Delta \approx 0.63$ in the vicinity of the Fermi surface (cf figure 3(a)), and this value is much larger than $T_K^{(0)}$. Under this condition [12], $T_K^{(R)} \approx \delta\left(\frac{T_K^{(0)}}{D_0}\right)^{t_L^2 \sin^2 k_n/t^2}$, and

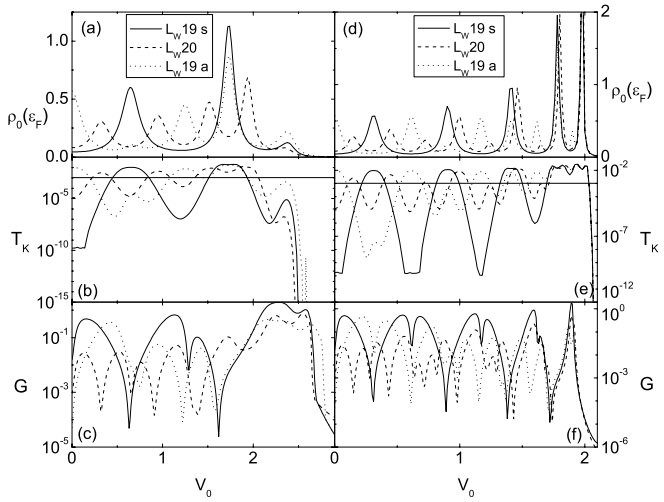

Figure 2. Variations of $\rho_s(\epsilon_F)$ ((a) and (d)), T_K ((b) and (e)) and G ((c) and (f)) versus V_0 for 'L_W19s' (solid), 'L_W20' (dashed) and 'L_W19a' (dotted). In (a)–(c), $L_B = 5$, and in (d)–(f), V_0 is constant over the whole wire. The other parameters are $t = 1$, $\epsilon_d = -0.7$, $U = 1.4$, $t_d = 0.5$, $t_L = 0.5$, $T = 10^{-3}$ and $\gamma = t_L^2/(2L_W)$. In (b) and (e), horizontal lines denote the T position.

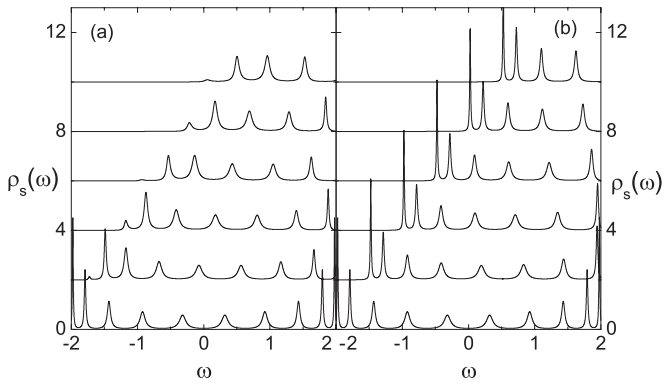

Figure 3. Evolution of $\rho_s(\omega)$ at zero temperature with $L_B = 5$ (a) and constant V_0 over the whole wire (b). From bottom to top, V_0 increases from zero to 2.5 with an interval 0.5. Each curve is offset by two units. $\gamma = t_L^2/(2L_W)$, with the same other parameters as in figure 2.

$T_K^{(NR)} \approx \Delta\left(\frac{T_K^{(0)}}{D_0}\right)^{t^2/(t_L^2 \sin^2 k_n)}$, with δ the half width at half maximum of the LDOS peak, which can also be obtained from figure 3(a) as $\delta \sim 0.059$. Consequently, $T_K^{(R)}$ and $T_K^{(NR)}$ calculated from the above analytic expressions are about 0.019 and 1.4×10^{-8}, respectively. (Here, $\sin k_n$ is assumed to be unity.) The corresponding T_K values estimated from our numeric results are in qualitative consistence with these analytic ones. These results prove the universal influence of the finite-size effect on the Kondo correlation, no matter whether the considered structure is an embedded or side-coupled QD system. Now, we focus our attention on the special characteristics of side-coupled QD structures.

In resonant regions, $|T_r|^2$ is close to unity in embedded QD structures, whereas it is close to zero in side-coupled QD structures, at finite temperature. Besides this well known difference [21], some new characteristics are found in side-coupled QD structures with the

symmetry broken. In the situation 'L_W20', the number of major resonant regions is doubled, from two to four, although L_W is only changed by one compared with the situation 'L_W19s'. In the third situation, the number of major resonant regions is also turned from two to four. In this situation, the wire length is even unchanged, and the only difference is the asymmetry introduced by the change of the dot position. The doubling of the number of resonant regions is a common characteristic of asymmetric structures. (As in 'L_W19s', a low peak of $\rho_s(\epsilon_F)$, and a shallow dip of G, can be found in $V_0 > 2$ in both of these two situations.) On the other hand, some difference can be found between these two asymmetric situations. In 'L_W20', the four major resonant regions are all located in the areas corresponding to the valleys of 'L_W19s', whereas in 'L_W19a', in the four major resonant regions, two appear in the same areas as the resonant regions of 'L_W19s', and the other two appear in the valleys of 'L_W19s'. The two sets of resonant regions of 'L_W20' and 'L_W19a' intersect with each other.

What is the underlying reason that accounts for the above symmetry-related phenomena? With $V_0 = 0$, if the wire is decoupled from the dot and disconnected from the leads, the energies and wavefunctions of eigenstates are $\epsilon_n = -2t\cos(k_n)$ and $\psi_n(i) = A_n \sin(k_n i)$, respectively, with $k_n = \pi n/(L_W+1)$ and A_n the renormalization factor. The energy separation between consecutive eigenstates is $2\pi t \sin(k_n)/(L_W+1)$, which is also the Δ value in the two asymmetric situations. However, in the situation 'L_W19s', $\Delta = 4\pi t \sin(k_n)/(L_W+1)$, because the wavefunction varies alternately between even and odd functions, and the site '10' is the node of odd functions. This halving of Δ can interpret the number doubling of resonant peaks. In figure 3(a), the evolution of $\rho_s(\omega)$ with V_0 is plotted for the situation 'L_W19s'. With V_0 increased, the $\rho_s(\omega)$ curve moves towards the positive ω direction, which yields a series of peaks in the $\rho_s(\epsilon_F)$–V_0 curve. Similar processes are also found in the two asymmetric situations. But since the peak number of the $\rho_s(\omega)$ curve is doubled, the resulting resonant region number of the $\rho_s(\epsilon_F)$–V_0 curve is also doubled.

As we have said, some difference can be found between the situations (ii) and (iii), although both of them are asymmetric. From $k_n = \pi n/(L_W+1)$, it can be seen that the energy levels of 'L_W19a' and 'L_W20' intersect with each other. This is reflected in the variations of $\rho_s(\omega)$, and consequently, $\rho_s(\epsilon_F)$, T_K and G. In the $\rho_s(\epsilon_F)$ curve of 'L_W19a', a new high peak is located at $V_0 = 0$, but the next peak is greatly suppressed compared with its counterpart in the symmetric structure. This can be understood easily from the eigenfunction form $\psi_n(i) = A_n \sin(k_n i)$. The eigenenergy level corresponding to $\epsilon_F = 0$ is $k_{10} = \pi/2$. Its two nearest-neighbour ones are $k_9 = 9\pi/20$ and $k_{11} = 11\pi/20$, which are close to $\pi/2$. At site 10 $|\sin(k_n i)|^2 = 1$ with $n = 9$ or 10, whereas at site 9 it is greatly reduced. This accounts for the suppression of the second peak in the $\rho_s(\epsilon_F)$–V_0 curve.

In figures 2(d)–(f), the variations of $\rho_s(\epsilon_F)$, T_K and G are given in the three situations under an external voltage which is constant over the whole wire. As expected, the resonant regions of the $\rho_s(\epsilon_F)$–V_0 curve have one-to-one correspondence with the T_K peaks. In these regions, the transport is Kondo assisted, and G shows deep dips. Out of these regions, intrinsic structures are found in G due to the scattering at the interfaces between the wire and leads. Here, the relation $T_K^{(NR)} \ll T \ll T_K^{(R)}$ is also satisfied. Compared with the results of $L_B = 5$, the number of resonant regions is increased. When V_0 exceeds two, the low $\rho_s(\epsilon_F)$ peak found in structures with $L_B = 5$ does not appear, and G decreases rapidly. In figure 3(b), the evolution of the $\rho_s(\omega)$ curve with V_0, which is constant over the whole wire, is plotted for the situation 'L_W19s'. As we can see from the comparison between figures 3(a) and (b), for the case with constant V_0 the curve moves almost rigidly, and when $V_0 > 2$ all of the original five peaks below $\omega = 0$ pass through the Fermi surface, which results in five peaks in the $\rho_s(\epsilon_F)$ curve. As V_0 further increases, the tunnelling through the wire is exponentially depressed, and G decreases rapidly. However, the case with $L_B = 5$ displays a different scenario. With V_0 increased, the $\rho_s(\omega)$

curve also moves towards the positive ω direction, but its speed is slow, and when $V_0 = 2$, some peaks have not passed the Fermi surface. Besides this, in the case with $L_B = 5$, the movement is not rigid. With V_0 increased, the left-most peak is diminished and removed, then the new left-most peak undergoes the same process, until all surviving peaks pass $\epsilon_F = 0$. As a result, in the $\rho_s(\epsilon_F)$ curve, only two major peaks appear, and the low peak originates from a diminished left-most peak in the evolution of the $\rho_s(\omega)$ curve. The difference between the cases with $L_B = 5$ and constant V_0 comes mainly from their different barrier widths. With the effective barrier width increased, the tunnelling above $V_0 = 2$ is exponentially diminished, the number of resonant regions is increased, and the results is more and more close to those with constant V_0.

In the $\rho_s(\omega)$ curve, the outmost peaks have narrower widths than the inmost ones. For example, $\delta = 0.0065$ in the left-most peak at $V_0 = 0$. This width is about one-tenth of the peak in the vicinity of the Fermi energy. However, the peak values of T_K in different resonant regions have the same order in magnitude. This explains why clusters with different sizes are used in calculation of T_K (or $\rho_s(\omega)$) and G.

4. Summary

In summary, we investigate the influence of an external voltage V_0 on conductance G through a QD, which is side-coupled to a quantum wire of length L_W, whose two ends are weakly connected to leads. To treat this problem, the PMSL and the SBMF method of KR are employed. With V_0 increased, a series of resonant regions is formed. If the relation $T_K^{(NR)} \ll T \ll T_K^{(R)}$ is satisfied, Kondo-assisted tunnelling leads to very small G values in resonant regions, whereas intrinsic structures of G are found in non-resonant regions due to scattering at interfaces between the wire and leads. This is the universal result of the finite-size effect on the Kondo correlation. Consider the situation where the wire contains an odd number of sites: if the QD is side-coupled to the symmetric site the would-be resonant regions corresponding to odd wavefunctions are removed, but if the dot is side-coupled to one other site the symmetry is broken and these regions are recovered. In two asymmetric structures with wire length L_W and $L_W + 1$, respectively, the two sets of resonant regions intersect with each other. These symmetry-related phenomena characterize side-coupled QD structures. With V_0 constant over the wire, the $\rho_s(\omega)$ curve moves rigidly. But if a potential barrier is formed in the wire, with its effective width being shorter than L_W, some peaks in the $\rho_s(\omega)$ curve are diminished and removed, so that the number of resonant regions is decreased.

Acknowledgments

The author Z-YZ acknowledges the support by National Foundation of Natural Science in China grant No 10204012, and by the Special Funds for Major State Basic Research project No G001CB3095 of China. S-JX acknowledges the support by National Foundation of Natural Science in China grant No 10074029, and by the China State Key Projects of Basic Research (G1999064509).

References

[1] Goldhaber-Gordon D, Shtrikman H, Mahalu D, Abusch-Magder D, Meirev U and Kaster M A 1998 *Nature* **391** 156

[2] Cronewett S M, Oosterkamp T H and Kouwenhoven L P 1998 *Science* **281** 540

[3] Simmel F, Blick R H, Kotthaus U P, Wegsheider W and Blichler M 1999 *Phys. Rev. Lett.* **83** 804
[4] van der Wiel W G, De Franceschi S, Fujisawa T, Elzerman J M, Tarucha S and Kouwenhoven L P 2000 *Science* **289** 2105
[5] Ji Y, Heiblum M, Sprinzak D, Mahalu D and Shtrikman H 2000 *Science* **290** 779
[6] Hewson A C 1993 *The Kondo Problem to Heavy Fermions* (Cambridge: Cambridge University Press)
[7] Kang K and Shin S-C 2000 *Phys. Rev. Lett.* **85** 5619
[8] Affleck I and Simon P 2001 *Phys. Rev. Lett.* **86** 2854
[9] Simon P and Affleck I 2001 *Phys. Rev.* B **64** 085308
[10] Hu H, Zhang G-M and Yu L 2001 *Phys. Rev. Lett.* **86** 5558
[11] Simon P and Affleck I 2002 *Phys. Rev. Lett.* **89** 206602
[12] Simon P and Affleck I 2003 *Phys. Rev.* B **68** 115304
[13] Sorensen E S and Affleck I 2005 *Phys. Rev. Lett.* **94** 086601
[14] Anderson P W 1970 *J. Phys. C: Solid State Phys.* **3** 2436
[15] Coleman P 1984 *Phys. Rev.* B **29** 3035
[16] Kotliar G and Ruckenstein A E 1986 *Phys. Rev. Lett.* **57** 1362
[17] Dorin V and Schlottmann P 1993 *Phys. Rev.* B **47** 5095
[18] Dong B and Lei X L 2002 *Phys. Rev.* B **65** 241304
[19] Zhang Z-Y, Xiong S-J and Evangelou B 1998 *J. Phys.: Condens. Matter* **10** 8049
[20] Meir Y, Hirose K and Wingreen N S 2002 *Phys. Rev. Lett.* **89** 196802
[21] Kang K, Cho S Y, Kim J J and Shin S C 2001 *Phys. Rev.* B **63** 113304